5

Determination of Chemical State and External Magnetic Field Effect on the Energy Shifts and X-Ray Intensity Ratios of Yttrium and Its Compounds

Sevil Porikli[1] and Yakup Kurucu[2]
Erzincan University, Faculty of Art and Sciences, Department of Physics
Atatürk University, Faculty of Sciences, Department of Physics
Turkey

1. Introduction

The term 'X-ray fluorescence analysis' (XRF) refers to the measurement of characteristic fluorescent emission resulting from the deexcitation of inner shell vacancies produced in the sample by means of a suitable source of radiation. For a particular energy (wavelength) of fluorescent light emitted by a sample, the number of photons per unit time (generally referred to as peak intensity or count rate) is related to the amount of that analyte in the sample. The counting rates for all detectable elements within a sample are usually calculated by counting, for a set amount of time, the number of photons that are detected for the various analytes' characteristic X-ray energy lines. It is important to note that these fluorescent lines are actually observed as peaks with a semi-Gaussian distribution because of the imperfect resolution of modern detector technology. Therefore, by determining the energy of the X-ray peaks in a sample's spectrum, and by calculating the count rate of the various elemental peaks, it is possible to qualitatively establish the elemental composition of the samples and to quantitatively measure the concentration of these elements.

XRF is an analytical method to determine the chemical composition of all kinds of materials. The materials can be in solid, liquid, powder, filtered or other form. XRF can also sometimes be used to determine the thickness and composition of layers and coatings. The method is fast, accurate and non-destructive, and usually requires only a minimum of sample preparation. Applications are very broad and include the metal, cement, oil, polymer, plastic and food industries, along with mining, mineralogy and geology, and environmental analysis is of water and waste materials. XRF is also a very useful analysis technique for research and pharmacy.

For routine XRF analysis, two major approaches are distinguishable based on the type of detector used to measure the characteristic X-ray emission spectra. Wavelength dispersive X-ray fluorescence (WDXRF) analyses depend upon the use of diffracting crystal to determine the characteristic wavelength of the emitted X-rays. Energy dispersive X-ray fluorescence (EDXRF) employs detectors that directly measure the energy of the X-rays by collecting the ionization produced in suitable detecting medium.

X-ray emission spectra are known to be influenced by chemical combination of X-ray emitting atoms with different ligands. The effect of the chemical combination, however are not large and a theoretical interpretation of these effects has not been established completely. Therefore, chemical effects have rarely been utilized in the characterization of materials. The purpose of this work was to study chemical effects and discuss their applications to Yttrium (Y) in various compounds. So much so that, this paper presents and discusses the measured spectra both energy dispersive and wave-length dispersive X-ray spectrometer. In the first part of the study, the effect of the 0.6T and 1.2T external magnetic field and chemical state on the *Ka*, $K\beta_{1,3}$ and $K\beta_{2,4}$ X-ray energies and relative intensity ratios for Y, YBr_3, YCl_3, YF_3, $Y(NO_3)_3.6H_2O$, Y_2O_3, YPO_4, $Y(SO_4)_3.8H_2O$ and Y_2S_3 have been investigated, using the 22.69 keV X-rays from a ^{109}Cd and 59.54 keV γ-ray from a ^{241}Am as photon sources. The measurements were done using an energy dispersive Si(Li) detector with photon excitation by radioisotopes. For B=0, the present experimental results were compared with the experimental and theoretical data in the literature.

The results show that Y_2O_3, YF_3 and Y_2S_3 can change owing to the applied magnetic field. In addition, we found that the energy of characteristic X-ray series is totally independent of the excitation source and mode. However, changes have been observed in X-ray spectra when the element studied in the sample is chemically bonded to others. The development of high resolution spectrometers allows for the characterization and study of these effects.

In the second part of the study, energies and full width at half maximum (FWHM) values of the *Ka*, $K\beta_{1,3}$ and $K\beta_{2,4}$ X-ray of Y and its compounds were measured by a wavelength dispersive spectrometer. An accurate analytical representation of each line, obtained by a fit to a minimal set of Gaussians, is presented. The absolute energies and FWHM values derived from the data, agree well with previous measurements. Possible origins of chemical shifts are discussed. It was found that the chemical shifts of Y *Ka* line in pure Y and its some compounds relatively small (less than 0.1 eV with pure Y as reference). The influence of crystal symmetry on the energy shifts of X-ray lines is an interesting aspect of our study. The results demonstrate a clear dependence of the energy shifts on the chemical state of the element in the sample. The relative intensities are more susceptible to the chemical environment than the energy shifts.

It is well known that the chemical environment of an element affects and modifies the various characteristics of its X-ray emission spectrum. Most of the works suffer from neglecting chemical influences, and usually theoretical atomic values (Scofield, 1974a, 1974b) are used as a reference even for quite different chemical compounds of certain element. However, some papers deal with chemical effects (Berenyi et al., 1978; Rao et al., 1986), mostly in connection with X-ray emission after an electron capture process (EC) and partially after photoionisation (PI). Paic &Pecar (1976) found that for first-row transition elements the $K\beta/Ka$ ratio depends on the mode of excitation. The difference between the ratios for electron-capture decay and photoionization becomes almost 10%. Similar results were obtained by Arndt et al., (1982) and they pointed out that the difference comes from a strong shake-off process accompanying photoionization.

The 3*d* transition metals have played an important role in the development of modern technology, and knowledge of their valence electronic structure is very important for understanding their physical properties. X-ray spectroscopy is an established tool for probing the electronic structure of 3*d* transition metal compounds (Meisel et al., 1989). A number of techniques, such as photoemission spectroscopy, X-ray absorption and X-ray emission spectroscopy create a hole in an inner shell in order to investigate the valance

electron configuration. Although some investigations have been made to study their electronic structures individually, no systematic study has been made so far for understanding the valence electronic structure of all the 3*d* transition metals. With a deeper theoretical understanding of the underlying processes and further improving X-ray sources, sophisticated experiments have been developed (e.g., resonant inelastic scattering, magnetic dichroism (Groot, 1994a,b)) that give detailed information on the valance electron configuration.

In a number of X-ray spectral studies of 3*d* transition metals it has been observed that the *Kβ*-to-*Kα* X-ray intensity ratios are dependent on the physical and chemical environments of the elements in the sample. In the earlier studies of 3*d* metal compounds (Küçüköder et al., 1993; Padhi et al., 1993, 1995), the influence of chemical effects has shown difference in the *Kβ*-to-*Kα* X-ray intensity ratios up to nearly 10%. Such chemical effects can be caused either by a varying 3*d* electron population or by the admixture of *p* states from the ligand atoms to the 3*d* states of the metal or both. Brunner et al. (1982) explained their experimental results by the change in screening of 3*p* electron by 3*d* valance electrons as well as the polarization effect. They also pointed out that the chemical effect is almost the same order of magnitude as the effect of excitation mode and both effects should be studied separately. However, most of these measurements have been performed with solid-state X-ray detectors and the change in the satellite peaks in the *Kβ* X-ray region has not been studied because of poor energy resolution. Urch (1979) discussed the chemical effect on the *K* X-ray spectra based on molecular-orbital (MO) theory. Similar studies on the chemical effect on the X-ray spectra have already been done extensively. However, these studies are concerned mostly on with transition energies and profiles of X-rays, and qualitative discussions on the intensities have not yet been made. Tamaki et al. (1979) studied Cr and 55Mn-labeled compounds and reported that the *Kβ*/*Kα* ratio increases with increasing formal oxidation number of the element in the compound. Kataria et al. (1986) found deviations of up to 10% for the same ratio in the case of Mn compounds. Mukoyama et al. (1986) experimentally confirmed the theoretical predictions following Brunners' (1982) model in the case of Te and Mo compounds for $K\beta_{1,3}$ and $K\beta_2$ components.

Wide employed applications and the intriguing asymmetry of the Cu Kα and Kβ line shapes (Deutsch&Hart, 1982) along with those of all 3d transition elements, led in turn to a century of extensive spectrometric studies of the Cu *Kα* and *Kβ* spectra. In spite of these extensive studied, recent studies reveal that surprises still lurk under the skewed $K\alpha_{1,2}$ and overlapping $K\beta_{1,3}$ lines, and the related multi-electronic satellite (S) and hypersatellite (HS) spectra. The asymmetric lineshape of the copper emission lines were attributed in the past to a number of different processes: Kondo-like interaction of the conduction electrons with the core holes, final state interactions between the core holes and the incomplete 3*d* shell, 2*p*/3*d* shell electrostatic exchange interaction, and most importantly, shake-up and shake-off of electrons from the 3*l* shells. The last process, in particular, received in the past strong experimental support.

Raj et al. (1998) were carried studies on CrB, CrB2 and FeB forms in order to look into the electronic structure of the transition metals in monoborides and diborides. In order to understand the valence electronic structure of the transition metals in the compounds, they have tried to compare the measured *Kβ*-to-*Kα* ratios with the multiconfiguration Dirac±Fock calculations assuming different electronic configurations for the transition metal. Such a comparison would provide information on the valence electronic structure of the transition metals in the compounds, which could in turn provide information on

the rearrangement of electrons between 3*d* and 4*s* states of the metal or electron transfer from the 3*d* state of the metal to the ligand atoms or vice-versa.

The chemical environment has a strong effect on the transitions originated in valence band and its influence could clearly be observed in the emission spectrum structure. The P-*Kβ* spectrum has been studied by many authors (Takashi, 1972; Taniguchi 1984; Torres Delluigi et al., 2003), who used both single-crystal and two-crystal spectrometers with conventional X-ray sources. These authors showed some modifications in the *Kβ* spectra and its relation with P chemical environment. Compounds with oxygen as ligand atom, a relationship between the ratio of the Kβ′ line intensity to the total intensity of the Kβ line and the energy shift of the Kα1,2 lines was found by them. Fichter (1975) discussed the *Ka*-line shifts related to the oxidation number of the P-atom. The chemical shift of X-ray emission lines is usually interpreted with the effective charges or oxidation number of the X-ray emitting atom (Leonhardt&Meisel, 1970; Meisel et al., 1989). For example, the Al *Ka* lines shift to higher energy in going from the metal to the oxide (Nagel et al., 1974). By comparing the measured chemical shifts with those of the reference compounds, Gohshi et al. (1973, 1975) determined the chemical state of S, Cr and Sn. They obtained not only qualitative, but also quantitative results.

Theoretical studies of emission spectra were performed mostly to study atoms with simple electronic configurations (see, e.g., the review by Mukoyama et. al., 2004). Theoretical calculations for solids and molecules have been done mainly to predict transition energies and line profiles, but evaluation of transition probabilities is rather scarce. This is due to two reasons: Firstly, molecular orbital methods and band theories are originally developed for ground states and sometimes difficult to apply to excited states with an inner-shell vacancy. Secondly, matrix elements for absorption and emission processes in molecules include multi-center integrations, which are tedious and require long computing times. Most individual authors indicate that their results favor the Dirac-Hartree-Fock calculations of Scofield (1974a), rather than the significantly lower predictions of the same author's earlier Dirac-Hartree-Slater calculations (Scofield, 1969). Both of these describe the de-excitation of a single *K* vacancy in a neutral atom. However careful examinations (Salem et al., 1974; Khan&Karimi, 1980) of all available data reveal a tendency for *Kβ*/*Ka* to fall somewhat below the DHF predictions in the atomic number region 21<Z<32 where the 3*d* subshell is filling.

Band et al. (1985) applied the scattered-wave (SW) X*a* MO method to calculate the chemical effect on the *Kβ*/*Ka* intensity ratios. They performed the MO calculations for different chemical compounds of Mn and Cr using the cluster method and obtained the spherically averaged self-consistent potential and the total charge of the valance electrons in the central atom region. Chemical effect on the *Kβ*/*Ka* X-ray intensity ratios or some Mn and Cr compounds has been studied both theoretically and experimentally by Mukoyama et al. (1986). The *K* X-ray spectra were measured by the use of a double crystal spectrometer with high energy resolution. The theoretical calculations were made with the use of the discrete-variational X*a* molecular-orbital method and the X-ray intensities were evaluated in the dipole approximation using molecular wave functions. Mukoyoma et al. (2000) have calculated the electronic structures of tetraoxo complexes of 4*d* and 5*d* elements with the discrete-variational *Xa* (DV-*Xa*) MO method. They found that the for Tc compounds, the calculated values were in good agreement with the measured values. In the case of Mo *K* X-rays, the agreement theory and experiment is not as good as with Tc compounds. Yamoto et

al. (1986) studied the variation of the relative *K* X-ray intensity ratios for compounds involving Tc isotopes, ^{95m}Tc, ^{97m}Tc and ^{99m}Tc. They found that the chemical effect on the $K\beta/Ka$ ratios for 4*d* elements is small but the dependence of the $K\beta_2/Ka$ ratios on the chemical environments is appreciable.

Mukoyoma et al. (1986) have calculated the $K\beta_2/Ka$ intensity ratios for chemical compounds of 4*d* transition elements by the use of the simple theoretical method of Brunner et al. (1982), originally developed for 3*d* elements. Although they obtained good agreement between theories and experimental, it was found that their model is inadequate for the metallic cases.

These investigations on the effect of 3*d* and 4*d* electrons were performed only to understand the chemical effect on the X-ray intensity ratios. However, if the dependence on the excitation mode is also caused by the difference in the number of 3*d* electrons, as shown in our previous work, both effects, i.e. the dependence on the chemical environment and on the excitation mode, can be treated simultaneously to estimate the $K\beta/Ka$ ratios in terms of the number of 3*d* electrons. However it may also be possible that these ratios are also expressed as a function of other parameters, such as bond length and effective number of 4*p* electrons. Considering these facts, it is interesting to study the dependence of the $K\beta_2/Ka$ ratio in 3*d* elements on various parameters of chemical compounds.

Iiahara et al. (1993) measured the *L* X-ray intensity ratios for some Nb and Mo compounds. When the measured $L\gamma_1/L\beta_1$ ratios were plotted as a function of the effective number of 4*d* electrons, they found that the experimental data are experimental data are almost on a straight line. However, it should be noted that the $4d\rightarrow2p$ transitions are allowed dipole transition and the 4d electron is the valance shell electron which participates directly in the X-ray emission. In this case the X-ray emission rate is proportional to the number of 4*d* electrons and increases with increasing effective number of 4*d* electrons.

The chemical behavior of actinide atoms (in particular, that of uranium) is determined by valance nl-electrons of three types: 7s, 6d and 5f. Although the bond energies of these electrons are almost equal, their wave-function differs greatly in distribution in the radial direction (Katz et al., 1986; Balasubramanian et al., 1994). It can be said that the 5f electrons have an only core arrangement in the atom. Therefore, when actinides chemical bonding is studied, several questions should be raised: (1) the possibility and form of 5f electrons participation in chemical bonding; (2) the necessity for taking into account the splitting of valance levels of the atom into two sublevels nl_+ and nl_- with total angular momentum $j=1\pm1/2$ because of the relativistic effect of spin-orbital splitting (SOS) (Pyykko,1988; Pepper et al., 1991); (3) the energetic stabilization of the specific chemical state of the heavy atom due to fine effects of electron density redistribution on valance orbital; (4) the possibility of independent participation of split subshells in chemical bond formation. One of the methods of modern precise spectroscopy capable of providing a correct description of chemical bonding process is the chemical shift (CS) method of X-ray emission lines, i.e. the change in their energy when the chemical state of the emitting atom is changed (Gohshi&Ohtsuka, 1973; Makarov, 1999; Batrakov et al., 2004).

Atomic theory has shown that the magnetic dipole moments observed in bulk matter arise from one or two origins: one is the motion of the electrons about their atomic nucleus (orbital angular momentum) and the other is the rotation of the electron about its own axis (spin angular momentum). The nucleus itself has a magnetic moment. Except in special types of experiments, this moment is so small that it can be neglected in the consideration of the usual macroscopic magnetic properties of bulk matter. When the atom is placed in an

external magnetic field, the magnetic field produces a torque on the magnetic dipole. The torque is tending to align the dipole with the field, associated with this torque; there is a potential energy of orientation:

$$\Delta E=-\mu_l B \quad (1)$$

μ_l is the orbital magnetic dipole moment of an electron. According to the quantum theory, all spectral lines arise from transitions of electrons between different allowed energy levels within the atom and the frequency of the spectral line is proportional to the energy difference between the initial and final levels. The slight difference in energy is associated with these different orientations in the magnetic field. In the presence of a magnetic field, the elementary magnetic dipoles, whether permanent or induced, will act to set up a field of induction of their own that will modify the original field.

Today investigations of magnetic effects on X-ray spectra became actual both from theoretical and experimental points of view. The numbers of works on this subject deal with magnetic circular dichroism (MCD) in X-ray absorption spectroscopy (XAS), that gives information on empty electron states in a valence band and their spin configurations (Thole et al., 1992, Stöhr&Wu, 1994). Several experiments have been performed on the external magnetic field effect on the *K* shell X-ray emission lines. Demir et al., (2006a) determined how the radiative transitions and the structures of the atoms in a strong magnetic field are affected, K*a* and K*β* X-ray production cross sections, the *K*-shell fluorescence yields and *I*(*Kβ/Ka*) intensity ratios for ferromagnetic Nd, Gd, and Dy and paramagnetic Eu and Ho were investigated using the 59.5 keV incident photon energy in the external magnetic fields intensities ± 0.75 T. On the other hand, Demir et al., (2006b) measured L_3 subshell fluorescence yields and level widths for Gd, Dy, Hg and Pb at 59.5 keV incident photon energy in the external magnetic field of intensities ± 0.75 T. Porikli et al. (2008a; 2008b; 2008c) conduct measurements using pure Ni, Co, Cu and Zn and their compounds. Characteristic quantities such as position of line maxima, full widths at half maximum (FWHM), indices of asymmetry and intensity ratio values were determined in the values of external magnetic field 0.6 T and 1.2 T. Several experiments have been performed on the external magnetic field effect on the *K* shell X-ray emission lines. Commonly, experimental *L* X-ray intensities are measured using radioisotopes as excitation sources (Han et al., 2010; Porikli, 2011b). They have the advantages of stable intensity and energy and of small sizes, which allow compact and efficient geometry, and they operate without any external power.

Our motivation in performing this experiment has been two fold. First, with the aim of a better understanding of the chemical effect and external magnetic field effect, we conduct measurements using pure yttrium (Y) and its compounds. Characteristic quantities such as position of line maxima, full widths at half maximum (FWHM), indices of asymmetry and $K\beta_1/Ka$, $K\beta_2/Ka$, $K\beta_2/K\beta_1$ and $K\beta/Ka$ intensity ratio values are determined in the values of external magnetic field 0.6 T and 1.2 T. In the present work, the measurements were done using a filtered 22.69 keV from Cd-109 and 59.54 keV from Am-241 point source and Si(Li) detector. Particle size effects were circumvented. Peak areas were determined using Gaussian fitting procedures and the errors in various corrections such as self-absorption and detector efficiency were minimized. The measured values were compared due to the external magnetic field and chemical effect. The measured values for B=0 were compared with other experimental and theoretical results. To our knowledge, these intensity ratio values of Y in the external magnetic field have not been reported in the literature and appear

to have been measured here for the first time. Secondly, spectra of *K* X-rays emitted from a Y target were measured in high resolution wave-length dispersive X-ray spectrometer (WDXRF). After the measurement, characteristic quantitative such as peak energy, indices of asymmetry, FWHM are determined. The measured spectra were described in terms of a background function (a straight line) and peaks having Gaussian profiles. The Microcal Orgin 7.5 was used for peak resolving and background subtraction of *K* X-rays.

2. Experimental

2.1 Experimental set up (EDXRF)

Yttrium compounds can serve as host lattices for doping with different lanthanide cations and they used as a catalyst for ethylene polymerization. As a metal, it is used on the electrodes of some high-performance spark plugs. Yttrium is also used in the manufacturing of gas mantles for propane lanterns as a replacement for thorium, which is radioactive. Developing uses include yttrium-stabilized zirconia in particular as a solid electrolyte and as an oxygen sensor in automobile exhaust systems. Yttrium is used in the production of a large variety of synthetic garnets. Small amounts of yttrium (0.1 to 0.2%) have been used to reduce the grain sizes of chromium, molybdenum, titanium, and zirconium. It is also used to increase the strength of aluminium and magnesium alloys. The addition of yttrium to alloys generally improves workability, adds resistance to high-temperature recrystallization and significantly enhances resistance to high-temperature oxidation (see graphite nodule discussion below).

The studied elements were Y, YBr_3, YCl_3, YF_3, $Y(NO_3)_3.6H_2O$, Y_2O_3, YPO_4, $Y(SO_4)_3.8H_2O$ and Y_2S_3. The purity of commercially obtained materials was better than 99%. For powdered samples, particle size effects have a strong influence on the quantitative analysis of infinitely thick specimens. Even for specimens of intermediate thickness, in which category the specimens analyzed in the present study fall, these effects can be significant. Therefore, to circumvent particle size effects all samples were grounded and sieved through a -400 mesh (<37 μm) sieve. The powder was palletized to a uniform thickness of 0.05-0.15 g cm^{-2} range by a hydraulic press using 10 ton in^{-2} pressure. The diameter of the pellet was 13 mm.

All of the lines were excited using a 100 mCi Am-241 annular radioactive source and Cd-109 point source of 10 mCi strength (providing $5.0x10^3$ $steradian^{-1}$ photon flux of Ag X-radiation). The fluorescent X-rays emitted from the targets were analyzed by a Si(Li) detector (effective area 12.5 mm^2, thickness 3 mm, Be window thickness 0.025 mm).

For each sample three separate measurements have been made just to see the consistency of the results obtained from different measurements agreed with a deviation of less than 1%. The experimental setup consist of a Si(Li) detector and Cd-109 radioactive source as shown in Fig. 1. The mechanical arrangement to house the source-sample-detector combination in a definite geometry was shown in Fig. 1. An Al, Pb conical collimator was used between the sample and the detector for the excitation to obtain a large beam of emergent radiation and to avoid the interaction of the X-rays emitted by the component elements of the radioactive capsule and detector.An Al, Pb conical collimator was used between the sample and the detector for the excitation to obtain a large beam of emergent radiation and to avoid the interaction of the X-rays emitted by the component elements of the radioactive capsule and detector. This collimator has an external diameter of 13 mm and it was placed in the internal diameter of the radioactive source (8 mm). A graded filter of Pb, Fe and Al to obtain a thin beam of photons scattered from the sample and to absorb undesirable radiation shielded the

detector. The sample-detector and excitation source-sample distances were optimized to get maximum count rate in the fluorescent peaks. The sample was placed approximately at 45° to the source-plane as well as to the detector-plane so that the intensity of scattered radiation could be minimized (Giauque et al., 1973). The count rate kept below 1000 counts s^{-1} in order to avoid peak broadening, energy shift and non-linearity. The data were collected into 16384 channels of a digital spectrum analyzer DSA-1000. The energy per channel was adjusted as 4 eV to determine the peak centroits and to discriminate the overlapped peaks. The samples were mounted in a sample holder placed between the pole pieces of an electromagnet capable of producing the magnetic field of approximately 2.66T at 2 mm pole range. During the study, the magnetic field intensities of, 0.6 T and 1.2 T were applied to the samples. An ammeter monitored the continuity and stability of the currents feeding the electromagnet. A typical *K* X-ray spectrum of Y at the 0.0 T, 0.6 T and 1.2 T is shown in Fig. 2. A typical *Ka*, $K\beta_{1,3}$ and $K\beta_{2,4}$ spectrum of Y, YBr_3, YCl_3, $Y(SO_4)_3.8H_2O$ and Y_2S_3 are shown in Fig. 3.

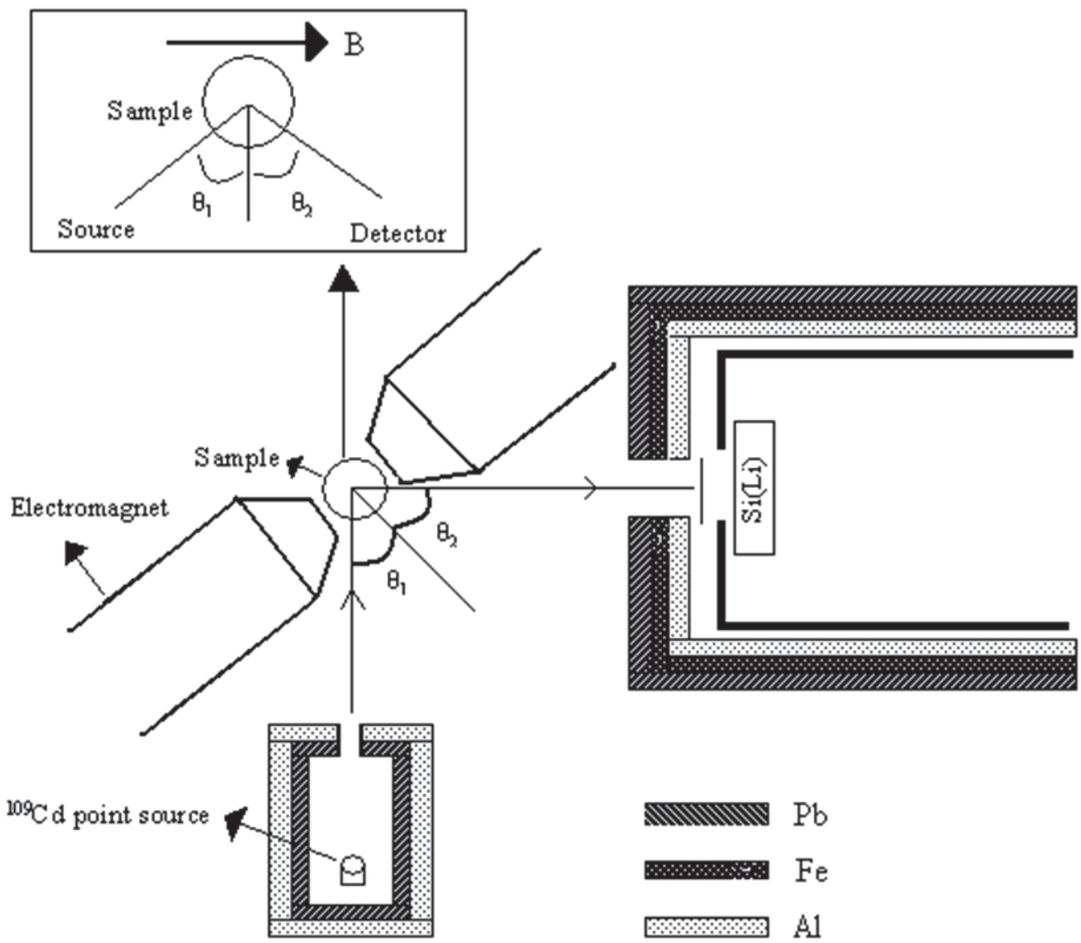

Fig. 1. Experimental set-up.

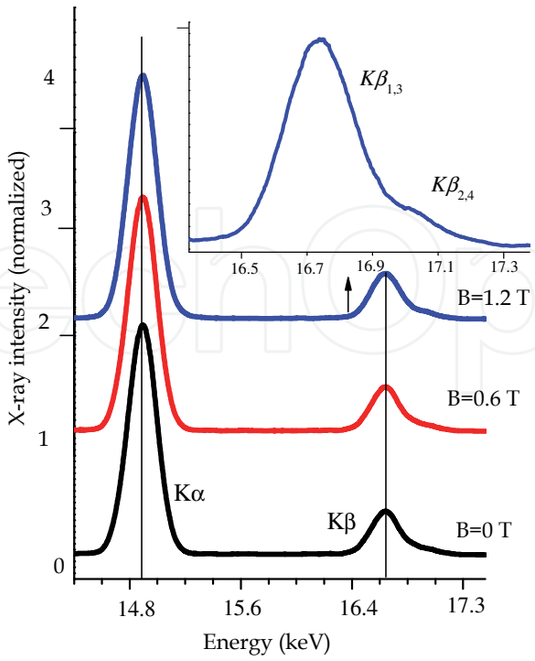

Fig. 2. A typical *K* X-ray spectrum of the Y target in B=0, B=0.6T and B=1.2 T magnetic field. The spectra were plotted after smoothing.

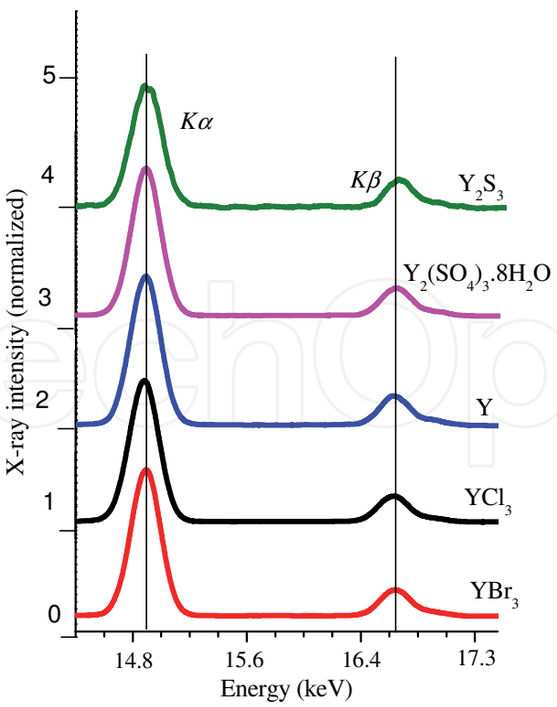

Fig. 3. Measured *Ka*, $K\beta_{1,3}$ and $K\beta_{2,4}$ spectra of Y, YBr_3, YCl_3, $Y(SO_4)_3.8H_2O$ and Y_2S_3. The spectra were plotted after smoothing.

Spectrum evaluation is a crucial step in X-ray analysis, as much as sample preparation and quantification. As with any analytical procedure, the final performance of X-ray analysis is determined by the weakest step in the process. The processing of ED spectra by means of computers has always been more evident because of their inherent digital nature. Due to relatively low resolving power of the employed Si(Li) detector, the process of evaluating XRF spectra is prone to many errors and requires dedicated software. For this purpose a software package called ORGIN was used for peak resolving background subtraction and determination of the net peak areas of *K* X-rays which is based on the non-linear least squares fitting of a mathematical model of the XRF spectrum.

2.2 Data analysis (EDXRF)

The $K\beta/Ka$ X-ray intensity ratio values have been calculated by using the relation

$$\frac{I(K\beta)}{I(K\alpha)} = \frac{N(K\beta)}{N(K\alpha)} \frac{\varepsilon(K\alpha)}{\varepsilon(K\beta)} \frac{\beta(K\alpha)}{\beta(K\beta)} \tag{2}$$

where $N(Ka)$ and $N(K\beta)$ are the net counts under the Ka and $K\beta$ peaks, respectively. $\beta(Ka)$ and $\beta(K\beta)$ are the self-absorption correction factor of the target and $\varepsilon(Ka)$ and $\varepsilon(K\beta)$ are the detector efficiency for Ka and $K\beta$ rays. The values of the factors, $I_0G\varepsilon$ which contain terms related to the incident photon flux, geometrical factor and the efficiency of the X-ray detector, were determined by collecting the Ka and $K\beta$ X-ray spectra of Ti, As, Br, Sr, Y, Zr and Ru with the mass thickness 0.02-0.17 g/cm² in the same geometry and calculated by using the following equation

$$I_0 G\varepsilon_{Ki} = \frac{N_{Ki}}{\sigma_{Ki}\beta_{Ki}t_i} \tag{3}$$

where N_{Ki} and β_{Ki} ($i=a, \beta$) have the same meaning as in Eq. (2). σ_{Ki} is X-ray fluorescence cross-section, G is a geometry factor and t is the mass of the sample in g/cm².

The self absorption correction factor β is calculated for both Ka and $K\beta$ separately by using the following expression

$$\beta_{Ki} = \frac{1-\exp\{-[\mu(E_0)\sec\theta_1 + \mu_{Ki}(E)\sec\theta_2]t\}}{[\mu(E_0)\sec\theta_1 + \mu_{Ki}(E)\sec\theta_2]t} \tag{4}$$

where $\mu(E_0)$ and $\mu_{Ki}(E)$ are the total mass absorption coefficients taken from WinXCOM programme which is the Windows version of XCOM. XCOM is the electronic version of Berger and Hubbell's Tables (Berger et al., 1987). The angles of incident photons and emitted X-rays with respect to the normal at the surface of the sample θ_1 and θ_2 were equal to 45° in the present setup.

The term σ_{Ki} represents the *K* X-ray fluorescence cross-sections and is given by

$$\sigma_{Ki} = \sigma_K^p w_K f_{Ki} \tag{5}$$

σ_K^p is the *K* shell photo ionization cross-section (Scofield, 1973), w_K is the fluorescence yield (Krause et al., 1979) and f_{Ki} is fractional X-ray emission rate (Scofield, 1974a).

2.3 Experimental set up (WDXRF)

A commercial WDXRF spectrometer (Rigaku ZSX 100e) was used for analysis of the different samples. This instrument is usually equipped with a 3 kW Rh-anode tube working at a voltage range of 20–50 kV and a current from 20 to 50 mA. It is possible to use primary beam filters (made of Zr, Al, Ti or Cu) between the primary radiation and the sample holder to reduce the background continuum and to improve the signal-to-noise ratio. Energy resolution and efficiency for each analytical line also depend on the collimator aperture and the analyzer crystal in use. Several different collimators can be used to reduce the step/scan resolution, as well as up to ten analyzer crystals, to better enhance spectral data for a specific element. Detection can be performed using a flow proportional counter (light elements) or a scintillation counter (heavy elements). In this work, analyses were made in vacuum atmosphere. Moreover, to avoid possible problems with inhomogeneity when measuring the samples, a sample spinner facility was used in all cases.

To investigate the spectrometer sensitivity in measuring of intensity and energy shift, one sample at same conditions was measured for three times. Because of the use of instruments such as sieve weight and hydraulic press, errors are caused in the results of analysis. These errors were called manual and instrumental errors. Three samples were prepared and measured for same conditions to determine these errors.

2.4 Spectral profile analysis (WDXRF)

The common method for evaluation of spectra in WDXRF is by the use of net peak line intensity. This is due to the high efficiency in the analytical results from the scintillation and/or the flow counter detectors. These detectors can receive up to 2×106 cps. In contrast, the common spectra evaluation in EDXRF is based on integration of the gross or net peak area due to a lower efficiency in the solid state detectors, usually limited to a maximum count of 5×104 cps. Taking into account these facts and to improve the sensitivity of the signal, the spectral data obtained by the WDXRF equipment were treated using the deconvolution software (Microcal Orgin 7.5), traditionally used in EDXRF spectrometry, to obtain the peak areas. The total number of counts increases considering the total peak area instead of only the analytical line. This leads also to an improvement of sensibility and detection limits. Once samples were analyzed, the identification of elements from the WDXRF spectra was done by using the qualitative scanning mode linked to the equipment, which includes automatic peak and element identification. The principle of WDXRF spectrometry is the use of different analyzer crystals to diffract and separate the different characteristic wavelengths of the elements present in the sample. For that reason, in WDXRF measurements, a multi-spectrum was obtained resulting from the use of different analyzing crystals, excitation conditions, etc.

Rigaku has improved their semi-quantitative software package further with the introduction of SQX. It is capable of automatically correcting for all matrix effects, including line overlaps. SQX can also correct for secondary excitation effect by photoelectrons (light and ultra-light elements), varying atmospheres, impurities and different sample sizes.

The obtained multispectra were split into the different individual spectra and were converted to energies by inversion of the channels to be treated using the means of the SQX software to perform spectral deconvolution and fitting and to evaluate element net peak areas from the spectra. Peak fitting was done by iteration to better adjust the peak and the background to minimize the chi-square of the fitting on each spectra. Fig. 4 shows the spectrum of Y. Measured numbers of counts are shown as solid black circles, while the red line represents the overall fit. The background is shown as a blue line.

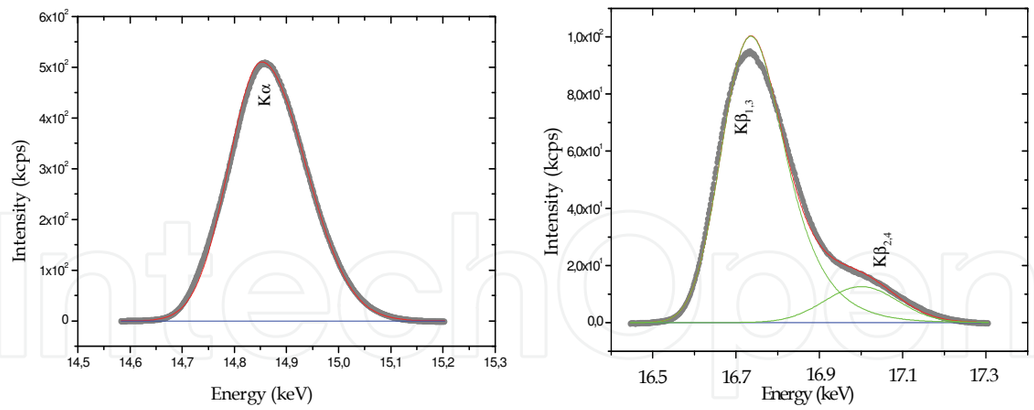

Fig. 4. Solid circles: Measured spectrum of Y *K* X-rays. Lines: Overall fitting function (red) and its components (green).

3. Results and discussion

A frequently used and convenient (but not very accurate) quantification of the line shape is by its full width at half maximum (FWHM) and index of asymmetry. These characteristics of lines (line parameters) are sensitive to change: line position (chemical shift), line shape (full width at half maximum (FWHM) and index of asymmetry) and additionally mutual ratios of line intensities. The peak position was determined at the center point of the 9/10 intensity of the smoothed line shape as illustrated in Fig. 5. It was known from our experience that the standard deviation of the peak position was determined using the peak top. Parameters such as FWHM and asymmetry index, defined in Fig. 5, were evaluated using the smoothed data. The Savitzky-Golay smoothing method was iteratively processed one time. Spectral smoothing was important for reducing the standard deviation of these parameters.

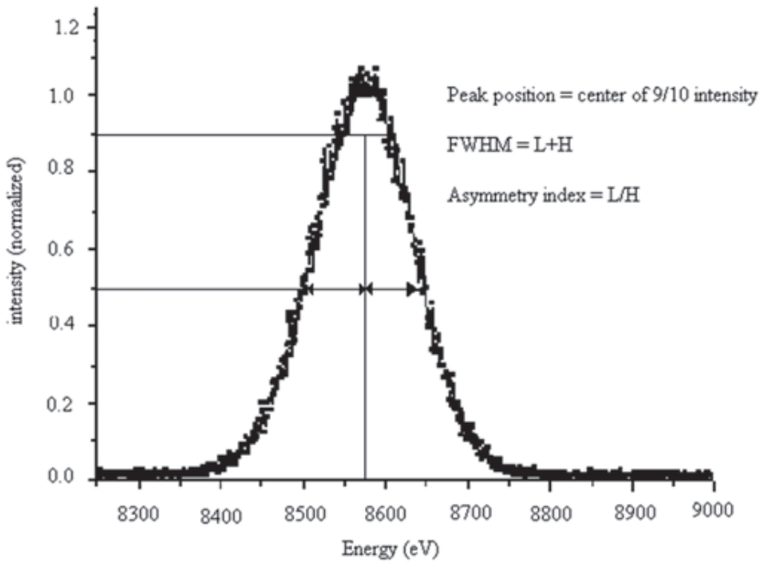

Fig. 5. Definition of asymmetry index, FWHM and peak position determined from 9/10 intensity.

The FWHM values for all compounds investigated for Cd-109 and Am-241 radioactive sources are given in Tables 1 and 2. Among all the Y compounds, the $Y(NO_3)_3.6H_2O$ *Ka* emission line shows large widths for both lines. Both the *Ka*, $K\beta_{1,3}$ and $K\beta_{2,4}$ lines become narrow when the compounds crystal system is monoclinic. In all cubic compounds such as Y_2O_3 and Y_2S_3 the lines FWHM values come closer to pure Y FWHM value. As can be seen from Table 1 and 2, for Zn compounds, the variation in the values of FWHM is relatively small. But when we compare the Y compounds with pure forms, we realize changes in both *Ka*, $K\beta_{1,3}$ and $K\beta_{2,4}$ FWHM values.

The nonmonotonic behavior of the *Ka* widths is probably due to the behavior of the *L* levels widths rather than the *K* level ones. The smaller overlap of the *M* and *K* wave functions, as compared to the *K* and *L* ones, may reduce the relative influence of possible similar sized nonmonotonic contributions originating in the final state level widths. Since experimental results FWHM and the index of asymmetry for B≠0 cannot be found in the literature, the comparison is not made with the other experimental values. As can be seen from Table 1 and 2, all FWHM values systematically decrease with increasing magnetic field intensity. Table 1 and 2 show that the experimental values of FWHM are unity within experimental uncertainties, suggesting the absence of chemical and external magnetic field effects.

Element	External Magnetic Field	Asymmetry Index (eV)			FWHM (eV)	
		Ka	$K\beta_{1,3}$	$K\beta_{2,4}$	*Ka*	$K\beta_{1,3}$
Y	**B=0**	**1.125**	**1.136**	**1.008**	**3.232**	**4.333**
	B=0.6T	1.079	1.112	1.006	3.223	4.268
	B=1.2T	0.991	0.109	0.996	3.057	4.016
$Y(NO_3)_3.6H_2O$	**B=0**	**1.122**	**1.127**	**1.011**	**3.211**	**4.228**
	B=0.6T	0.997	1.103	1.009	3.170	4.220
	B=1.2T	0.968	1.002	0.994	3.109	4.103
YCl_3	**B=0**	**1.110**	**1.119**	**0.994**	**3.197**	**4.267**
	B=0.6T	1.017	1.077	0.991	3.133	4.209
	B=1.2T	0.984	1.004	0.985	3.110	4.111
YPO_4	**B=0**	**1.114**	**1.111**	**0.987**	**3.199**	**4.337**
	B=0.6T	0.983	1.071	0.967	3.139	4.259
	B=1.2T	0.980	1.002	0.956	3.062	4.058
YBr_3	**B=0**	**1.098**	**1.078**	**0.971**	**3.201**	**4.284**
	B=0.6T	1.007	1.006	0.970	3.187	4.065
	B=1.2T	1.000	0.989	0.944	3.110	3.943
Y_2O_3	**B=0**	**1.071**	**1.05**	**0.938**	**3.266**	**4.121**
	B=0.6T	1.010	1.001	0.930	3.133	4.043
	B=1.2T	0.994	0.983	0.915	3.109	3.997
YF_3	**B=0**	**1.099**	**1.077**	**0.933**	**3.245**	**4.264**
	B=0.6T	1.022	1.011	0.929	3.120	4.001
	B=1.2T	0.988	0.984	0.886	3.100	3.966
$Y(SO_4)_3.8H_2O$	**B=0**	**1.055**	**1.035**	**0.921**	**3.189**	**4.166**
	B=0.6T	1.003	1.004	0.917	3.166	3.976
	B=1.2T	0.969	0.966	0.910	3.037	3.874
Y_2S_3	**B=0**	**1.024**	**1.031**	**0.910**	**3.337**	**4.494**
	B=0.6T	1.012	0.994	0.883	3.266	4.441
	B=1.2T	0.985	0.981	0.867	3.190	4.284

Table 1. Full width at half maximum (FWHM) and asymmetry index values of *Ka*, $K\beta_{1,3}$ and $K\beta_{2,4}$ emission lines in Y compounds for Cd-109 radioactive source.

To obtain more definite conclusions on FWHM dependency of the external magnetic field, more experimental data are clearly needed. The experimental uncertainties are always <0.05 eV for the FWHM.

According to Allinson (1933), the index of asymmetry of an X-ray emission line is defined as the ratio of the part of the FWHM lying to the long-wavelength side of the maximum ordinate to that on the short-wavelength side. In Table 1 and 2, the index of asymmetry for *Ka*, $K\beta_{1,3}$ and $K\beta_{2,4}$ emission lines are presented. The experimental uncertainties in the values cited in the table were determined taking into account multiple measurements and multiple fits of each spectrum. The errors for the index of asymmetry are ≤0.1 eV for *Ka*, $K\beta_{1,3}$ and $K\beta_{2,4}$.

Element	External Magnetic Field	Asymmetry Index (eV)			FWHM (eV)	
		Ka	$K\beta_{1,3}$	$K\beta_{2,4}$	*Ka*	$K\beta_{1,3}$
Y	**B=0**	**1.120**	**1.113**	**1.022**	**3.229**	**4.297**
	B=0.6T	1.089	1.100	1.016	3.212	4.203
	B=1.2T	1.009	0. 989	0.984	3.050	4.100
$Y(NO_3)_3.6H_2O$	**B=0**	**1.113**	**1.110**	**1.020**	**3.114**	**4.116**
	B=0.6T	1.028	1.104	1.013	3.017	4.111
	B=1.2T	0.996	0.993	1.001	3.091	4.075
YCl_3	**B=0**	**1.109**	**1.105**	**1.017**	**3.077**	**4.122**
	B=0.6T	1.003	1.007	1.009	3.041	4.110
	B=1.2T	0.978	0.987	0.987	3.000	4.004
YPO_4	**B=0**	**1.111**	**1.075**	**0.993**	**3.201**	**4.177**
	B=0.6T	0.989	1.032	0.984	3.126	4.170
	B=1.2T	0.969	1.008	0.953	3.013	4.005
YBr_3	**B=0**	**1.101**	**1.031**	**0.988**	**3.421**	**4.136**
	B=0.6T	1.017	1.004	0.980	3.234	4.065
	B=1.2T	0.994	0.971	0.965	3.048	3.993
Y_2O_3	**B=0**	**1.056**	**1.006**	**0.974**	**3.555**	**4.008**
	B=0.6T	1.031	0.999	0.972	3.229	3.989
	B=1.2T	0.987	0.977	0.954	3.096	3.974
YF_3	**B=0**	**1.077**	**1.001**	**0.970**	**3.301**	**4.123**
	B=0.6T	1.005	0.984	0.954	3.137	4.012
	B=1.2T	0.993	0.975	0.950	3.009	3.940
$Y(SO_4)_3.8H_2O$	**B=0**	**1.064**	**0.991**	**0.964**	**3.202**	**4.109**
	B=0.6T	1.001	0.990	0.966	3.113	3.989
	B=1.2T	0.978	0.946	0.956	3.074	3.866
Y_2S_3	**B=0**	**1.011**	**0.995**	**0.949**	**3.441**	**4.301**
	B=0.6T	1.010	0.994	0.937	3.368	4.039
	B=1.2T	0.974	0.961	0.921	3.222	3.974

Table 2. Full width at half maximum (FWHM) and asymmetry index values of *Ka*, $K\beta_{1,3}$ and $K\beta_{2,4}$ emission lines in Y compounds for Am-241 radioactive source.

When the crystal system of Y compounds is cubic, the *Ka* emission lines are almost symmetric for $Y_2O_3$and Y_2S_3. It is clear from results that, except for Y and $Y(NO_3)_3.6H_2O$,the asymmetry are generally larger for the *Ka* peak. So we can say that, the line shapes of *Ka* are not symmetric. It is also found from the Table 2, when the crystal system of Y compounds is trigonal (YBr_3), the *Ka*, $K\beta_{1,3}$ and $K\beta_{2,4}$ emission lines are almost symmetric too. For Am-241, line shapes are more symmetric than the Cd-109. As seen from Table 1 and 2, in the presence of an external magnetic field, the asymmetry index of the Y compounds change. The *Ka*, $K\beta_{1,3}$ and $K\beta_{2,4}$ emission lines asymmetry indices values decrease with external magnetic field. However, a more asymmetric structure is encountered for the elements of which their crystal symmetry is cubic. Also, it is observed that monoclinic group is more symmetric than the others.

Element	**External Magnetic Field**	**Chemical shift (ΔE) (eV)**			**Energy shift (δE) (eV)**		
		Ka	$K\beta_{1,3}$	$K\beta_{2,4}$	*Ka*	$K\beta_{1,3}$	$K\beta_{2,4}$
Y	**B=0**	**0**	**0**	**0**	**0**	**0**	**0**
	B=0.6T				0.074	0.109	0.101
	B=1.2T				0.161	0.260	0.237
$Y(NO_3)_3.6H_2O$	**B=0**	**-0.333**	**-0.441**	**-0.216**	**0**	**0**	**0**
	B=0.6T				0.086	0.098	0.115
	B=1.2T				0.141	0.137	0.227
YCl_3	**B=0**	**-0.238**	**-0.309**	**-0.115**	**0**	**0**	**0**
	B=0.6T				0.481	0.235	0.288
	B=1.2T				0.612	0.368	0.339
YPO_4	**B=0**	**-0.121**	**-0.235**	**-0.103**	**0**	**0**	**0**
	B=0.6T				0.335	0.279	0.336
	B=1.2T				0.455	0.355	0.399
YBr_3	**B=0**	**-0.033**	**-0.065**	**-0.065**	**0**	**0**	**0**
	B=0.6T				0.444	0.131	0.338
	B=1.2T				0.657	0.4	0.551
Y_2O_3	**B=0**	**0.135**	**0.017**	**0.056**	**0**	**0**	**0**
	B=0.6T				0.111	0.124	0.543
	B=1.2T				0.185	0.303	0.441
YF_3	**B=0**	**0.164**	**0.191**	**0.198**	**0**	**0**	**0**
	B=0.6T				0.167	0.166	0.112
	B=1.2T				0.533	0.529	0.144
$Y(SO_4)_3.8H_2O$	**B=0**	**0.609**	**0.387**	**0.33**	**0**	**0**	**0**
	B=0.6T				0.089	0.12	0.051
	B=1.2T				0.354	0.293	0.237
Y_2S_3	**B=0**	**0.899**	**0.872**	**0.808**	**0**	**0**	**0**
	B=0.6T				0.173	0.204	0.206
	B=1.2T				0.199	0.307	0.333

Table 3. Chemical shift (ΔE) and energy shift (δE) values of *Ka,* $K\beta_{1,3}$ and $K\beta_{2,4}$ emission lines in Y compounds for Cd-109 radioactive source.

The more unpaired 3d or 4d electrons the atom possesses, the more asymmetric will be the line observed. This kind observation led Tsutsumi (1959) to consider that the interaction between the hole created in the $2p_{3/2}$ or $2p_{1/2}$ shell (due to the transition of an electron from this shell to the 1s level) and the electrons in the incomplete 3d shell in the transition metal atoms is responsible for asymmetric nature of *Ka* lines. They proposed a theoretical model based on this idea to account for the asymmetry in the X-ray emission lines in the firs-row transition metal compounds. However, this is not the only consideration which can explain the origin of the asymmetry of the line; there are other considerations which are based on the relaxation effect of the inner state proposed by Parratt (1959) or on the interactions between 2p hole and electrons in the Fermi sea as proposed by Doniach and Sunjic (1970).

Element	**External Magnetic Field**	**Chemical shift (ΔE) (eV)**			**Energy shift (δE) (eV)**		
		Ka	$K\beta_{1,3}$	$K\beta_{2,4}$	*Ka*	$K\beta_{1,3}$	$K\beta_{2,4}$
Y	**B=0**	**0**	**0**	**0**	**0**	**0**	**0**
	B=0.6T				0.125	0.121	0.132
	B=1.2T				0.179	0.219	0.269
$Y(NO_3)_3.6H_2O$	**B=0**	**-0.401**	**-0.347**	**-0.316**	**0**	**0**	**0**
	B=0.6T				0.091	0.111	0.158
	B=1.2T				0.104	0.169	0.201
YCl_3	**B=0**	**-0.023**	**-0.109**	**-0.153**	**0**	**0**	**0**
	B=0.6T				0.226	0.254	0.259
	B=1.2T				0.559	0.472	0.318
YPO_4	**B=0**	**0.231**	**0.304**	**0.221**	**0**	**0**	**0**
	B=0.6T				0.553	0.602	0.436
	B=1.2T				0.598	0.556	0.511
YBr_3	**B=0**	**-0.133**	**-0.227**	**-0.194**	**0**	**0**	**0**
	B=0.6T				0.342	0.313	0.387
	B=1.2T				0.600	0.499	0.458
Y_2O_3	**B=0**	**0.440**	**0.316**	**0.241**	**0**	**0**	**0**
	B=0.6T				0.447	0.423	0.505
	B=1.2T				0.682	0.613	0.553
YF_3	**B=0**	**0.206**	**0.391**	**0.190**	**0**	**0**	**0**
	B=0.6T				0.367	0.276	0.211
	B=1.2T				0.533	0.590	0.438
$Y(SO_4)_3.8H_2O$	**B=0**	**0.194**	**0.276**	**0.133**	**0**	**0**	**0**
	B=0.6T				0.194	0.146	0.115
	B=1.2T				0.402	0.281	0.296
Y_2S_3	**B=0**	**0.575**	**0.503**	**0.421**	**0**	**0**	**0**
	B=0.6T				0.197	0.340	0.247
	B=1.2T				0.331	0.349	0.366

Table 4. Chemical shift (ΔE) and energy shift (δE) values of *Ka,* $K\beta_{1,3}$ and $K\beta_{2,4}$ emission lines in Y compounds for Am-241 radioactive source.

The chemical shift was the difference between the center point of the 9/10 peak intensity of a compound and that of pure Y measured before and after the measurement of the compound. When the environment of the emitting atom is changed, there are changes in the position of emission lines with respect to those in the pure metal. These changes are called chemical shifts. They are presented in Tables 3 and 4. Both the 4*d* electron configuration and crystal structure affect the chemical shift and energy shift with applied external magnetic field. There is a clear relationship with the external magnetic field values and the energy shift values of Y compounds, as is found in Table 3 and 4's last column. For higher values of external magnetic field, the values of energy shift increases systematically. But we do not find any relationship between external magnetic field and crystal structure of the compound. To obtain more definite conclusion, more experimental data for 4*d* compounds which crystal structure different are needed.
The errors of the chemical and energy shifts, originate mainly from the limited precision of our measurements, determined by repetitive measurements of all pure targets, which were prepared and placed in the same experimental geometry. The precision in the position of *Ka*, $K\beta_{1,3}$ and $K\beta_{2,4}$ lines was determined as 0.05 eV, whereas the maximum deviation of a single measurement from the average value was 0.1 eV.

Element	**Differences between FWHM values [ΔFWHM=FWHM$_{com.}$-FWHM$_{pure}$] (eV)**			**Chemical shift (ΔE) (eV)**		
	Ka	$K\beta_{1,3}$	$K\beta_{2,4}$	*Ka*	$K\beta_{1,3}$	$K\beta_{2,4}$
Y	0	0	0	0	0	0
$Y(NO_3)_3.6H_2O$	0.155	0.031	0.012	0.132	0.126	0.125
YCl_3	0.091	0.058	0.033	0.268	0.238	0.284
YPO_4	-0.223	-0.087	-0.107	-0.454	-0,444	-0.415
YBr_3	0.114	0.071	0.067	0.144	0.179	0.156
Y_2O_3	-0.077	-0.068	-0.021	-0.096	-0.126	-0.085
YF_3	-0.095	-0.034	-0.048	-0.115	-0.127	-0.167
$Y(SO_4)_3.8H_2O$	0.054	0.023	0.181	0.183	0.145	0.106
Y_2S_3	-0.013	-0.064	-0.079	-0.301	-0.397	-0.385

Table 5. Chemical shift *(ΔE)* and differences between FWHM values of *Ka,* $K\beta_{1,3}$ and $K\beta_{2,4}$ emission lines in Y compounds obtained for WDXRF.

It is also seen from Table 5 that the *Ka* line width of YPO_4 compound is wider than that of the other compounds. Compare with the *Ka* peak of the pure Y, that of cubic crystal structure Yttrium compounds shifted to lower energy, and the peak shift ordering was $YF_3<Y_2O_3<Y_2S_3<YPO_4$. The line shapes of *Ka* are generally symmetric. Y_2S_3 and Y_2O_3, where the $K\beta_{1,3}$ and $K\beta_{2,4}$ peak shifts are large, show prominent asymmetry.
The accurate knowledge of the $K\beta_1/Ka$, $K\beta_2/Ka$, $K\beta_2/K\beta_1$ and $K\beta/Ka$ intensity ratios is required for a number of practical applications of X-rays, e.g. molecular and radiation physics investigations, in non-destructive testing, elemental analysis, medical research etc. Therefore, these ratios depend sensitively on the atomic structure. Thus they have been widely used also for critical evaluation of atomic structure model calculations. We now discuss the values of these ratios as obtained in our measurements.
The relevant information in a spectrum is contained in its peaks whose position and area are linked respectively to the photon energy and the activity of the connected radionuclide. The peak areas can also be used to determine emission probabilities. In this work, peak areas

were determined after the Ka, $K\beta_{1,3}$ and $K\beta_{2,4}$ areas were separated by fitting the measured spectra with multi-Gaussian function plus polynomial backgrounds using Microcal Orgin 7.5 software program. Details of the experimental set up and data analysis have been reported earlier (Porikli et al., 2011b).

Table 6 lists the theoretical values which were calculated by Scofield (Scofield 1974a; Scofield, 1974b). Addition to this, the measured values of the $K\beta_1/Ka$, $K\beta_2/Ka$, $K\beta_2/K\beta_1$ and $K\beta/Ka$ intensity ratios in Y, and previous experimental and the other theoretical values of these ratios for pure elements and their compounds are listed in Table 6.

Element	External Magnetic Field	Intensity Ratio	This Work	Scofield (1974a)	Manson &Kennedy (1974)	Ertuğral et al. (2007)
Y	**B=0**	$K\beta_{1,3}/Ka$	0.2307±0.010	0.22910		
		$K\beta_{2,4}/Ka$	0.0317±0.008	0.02902		
		$K\beta_{2,4}/K\beta_{1,3}$	0.1981±0.011	0.19220		
		$K\beta/Ka$	**0.1822±0.008**	**0.16960**	**0.1685**	**0.1856±0.009**
	B=0.6T	$K\beta_{1,3}/Ka$	0.2289±0.007			
		$K\beta_{2,4}/Ka$	0.0311±0.008			
		$K\beta_{2,4}/K\beta_{1,3}$	0.1956±0.011			
		$K\beta/Ka$	**0.1753±0.011**			
	B=1.2T	$K\beta_{1,3}/Ka$	0.2275±0.007			
		$K\beta_{2,4}/Ka$	0.0304±0.008			
		$K\beta_{2,4}/K\beta_{1,3}$	0.1941±0.011			
		$K\beta/Ka$	**0.1712±0.011**			
$Y(NO_3)_3.6H_2O$	**B=0**	$K\beta_{1,3}/Ka$	0.2339±0.008			
		$K\beta_{2,4}/Ka$	0.0325±0.010			
		$K\beta_{2,4}/K\beta_{1,3}$	0.1987±0.011			
		$K\beta/Ka$	**0.1829±0.006**			
	B=0.6T	$K\beta_{1,3}/Ka$	0.2320±0.008			
		$K\beta_{2,4}/Ka$	0.0316±0.008			
		$K\beta_{2,4}/K\beta_{1,3}$	0.1977±0.010			
		$K\beta/Ka$	**0.1796±0.011**			
	B=1.2T	$K\beta_{1,3}/Ka$	0.2315±0.008			
		$K\beta_{2,4}/Ka$	0.0310±0.011			
		$K\beta_{2,4}/K\beta_{1,3}$	0.1954±0.011			
		$K\beta/Ka$	**0.1742±0.010**			
YCl_3	**B=0**	$K\beta_{1,3}/Ka$	0.2341±0.010			
		$K\beta_{2,4}/Ka$	0.0329±0.008			
		$K\beta_{2,4}/K\beta_{1,3}$	0.1992±0.009			
		$K\beta/Ka$	**0.1836±0.010**			
	B=0.6T	$K\beta_{1,3}/Ka$	0.2337±0.006			
		$K\beta_{2,4}/Ka$	0.0305±0.009			
		$K\beta_{2,4}/K\beta_{1,3}$	0.1952±0.009			

Element	External Magnetic Field	Intensity Ratio	This Work	Scofield (1974a)	Manson &Kennedy (1974)	Ertuğral et al. (2007)
		$K\beta/Ka$	**0.1821±0.011**			
	B=1.2T	$K\beta_{1,3}/Ka$	0.2322±0.010			
		$K\beta_{2,4}/Ka$	0.0324±0.008			
		$K\beta_{2,4}/K\beta_{1,3}$	0.1972±0.009			
		$K\beta/Ka$	**0.1818±0.010**			
YPO_4	**B=0**	$K\beta_{1,3}/Ka$	0.2355±0.010			
		$K\beta_{2,4}/Ka$	0.0333±0.010			
		$K\beta_{2,4}/K\beta_{1,3}$	0.1999±0.010			
		$K\beta/Ka$	**0.1840±0.009**			
	B=0.6T	$K\beta_{1,3}/Ka$	0.2336±0.007			
		$K\beta_{2,4}/Ka$	0.0320±0.009			
		$K\beta_{2,4}/K\beta_{1,3}$	0.1966±0.011			
		$K\beta/Ka$	**0.1773±0.008**			
	B=1.2T	$K\beta_{1,3}/Ka$	0.2322±0.011			
		$K\beta_{2,4}/Ka$	0.0304±0.009			
		$K\beta_{2,4}/K\beta_{1,3}$	0.1693±0.009			
		$K\beta/Ka$	**0.1738±0.011**			
YBr_3	**B=0**	$K\beta_{1,3}/Ka$	0.2359±0.008			
		$K\beta_{2,4}/Ka$	0.0341±0.007			
		$K\beta_{2,4}/K\beta_{1,3}$	0.2004±0.009			
		$K\beta/Ka$	**0.1848±0.010**			
	B=0.6T	$K\beta_{1,3}/Ka$	0.2342±0.008			
		$K\beta_{2,4}/Ka$	0.0321±0.009			
		$K\beta_{2,4}/K\beta_{1,3}$	0.1987±0.010			
		$K\beta/Ka$	0.1818±0.010			
	B=1.2T	$K\beta_{1,3}/Ka$	0.2321±0.009			
		$K\beta_{2,4}/Ka$	0.0303±0.011			
		$K\beta_{2,4}/K\beta_{1,3}$	0.1976±0.010			
		$K\beta/Ka$	0.1794±0.009			
Y_2O_3	**B=0**	$K\beta_{1,3}/Ka$	0.2364±0.011			
		$K\beta_{2,4}/Ka$	0.0349±0.010			
		$K\beta_{2,4}/K\beta_{1,3}$	0.2008±0.010			
		$K\beta/Ka$	0.1856±0.011			
	B=0.6T	$K\beta_{1,3}/Ka$	0.2351±0.008			
		$K\beta_{2,4}/Ka$	0.0340±0.008			
		$K\beta_{2,4}/K\beta_{1,3}$	0.1998±0.010			
		$K\beta/Ka$	0.1831±0.010			
	B=1.2T	$K\beta_{1,3}/Ka$	0.2302±0.010			
		$K\beta_{2,4}/Ka$	0.0307±0.010			
		$K\beta_{2,4}/K\beta_{1,3}$	0.1985±0.010			

Element	External Magnetic Field	Intensity Ratio	This Work	Scofield (1974a)	Manson &Kennedy (1974)	Ertuğral et al. (2007)
		$K\beta/Ka$	0.1824±0.009			
YF_3	**B=0**	$K\beta_{1,3}/Ka$	0.2371±0.008			
		$K\beta_{2,4}/Ka$	0.0352±0.009			
		$K\beta_{2,4}/K\beta_{1,3}$	0.2011±0.010			
		$K\beta/Ka$	0.1859±0.010			
	B=0.6T	$K\beta_{1,3}/Ka$	0.2338±0.006			
		$K\beta_{2,4}/Ka$	0.0330±0.008			
		$K\beta_{2,4}/K\beta_{1,3}$	0.2003±0.011			
		$K\beta/Ka$	0.1841±0.010			
	B=1.2T	$K\beta_{1,3}/Ka$	0.2307±0.009			
		$K\beta_{2,4}/Ka$	0.0325±0.010			
		$K\beta_{2,4}/K\beta_{1,3}$	0.1989±0.011			
		$K\beta/Ka$	0.1829±0.011			
$Y(SO_4)_3.8H_2O$	**B=0**	$K\beta_{1,3}/Ka$	0.2380±0.007			
		$K\beta_{2,4}/Ka$	0.0355±0.012			
		$K\beta_{2,4}/K\beta_{1,3}$	0.2015±0.010			
		$K\beta/Ka$	0.1867±0.011			
	B=0.6T	$K\beta_{1,3}/Ka$	0.2323±0.008			
		$K\beta_{2,4}/Ka$	0.0332±0.012			
		$K\beta_{2,4}/K\beta_{1,3}$	0.2006±0.011			
		$K\beta/Ka$	0.1844±0.012			
	B=1.2T	$K\beta_{1,3}/Ka$	0.2311±0.007			
		$K\beta_{2,4}/Ka$	0.0318±0.012			
		$K\beta_{2,4}/K\beta_{1,3}$	0.2001±0.010			
		$K\beta/Ka$	0.1816±0.011			
Y_2S_3	**B=0**	$K\beta_{1,3}/Ka$	0.2385±0.012			
		$K\beta_{2,4}/Ka$	0.0359±0.009			
		$K\beta_{2,4}/K\beta_{1,3}$	0.2019±0.009			
		$K\beta/Ka$	0.1876±0.008			
	B=0.6T	$K\beta_{1,3}/Ka$	0.2354±0.007			
		$K\beta_{2,4}/Ka$	0.0335±0.010			
		$K\beta_{2,4}/K\beta_{1,3}$	0.2009±0.009			
		$K\beta/Ka$	0.1867±0.011			
	B=1.2T	$K\beta_{1,3}/Ka$	0.2332±0.006			
		$K\beta_{2,4}/Ka$	0.0301±0.007			
		$K\beta_{2,4}/K\beta_{1,3}$	0.2002±0.008			
		$K\beta/Ka$	0.1849±0.012			

Table 6. $K\beta_{1,3}/Ka$, $K\beta_{2,4}/Ka$, $K\beta_{2,4}/K\beta_{1,3}$ and $K\beta/Ka$ X-ray intensity ratios of pure Y their compounds.

When you look at the Table 6, a serious difference between the $K\beta_{1,3}/Ka$ experimental and theoretical values can be seen. This situation is mainly because of the limited resolution of the detector. The Ka_1 and Ka_2 X-ray components appear as one line. In the most general case, chemical speciation is preferably performed via the analysis of the $K\beta_{1,3}$ or $K\beta_{2,4}$ lines. These lines, emitted after transition of valance electrons are more sensitive to the chemical environment.

As can be seen from Table 6, the $K\beta/Ka$ ratios of Y in all Y compounds are in close agreement with the ratios of corresponding pure metals. The greatest increase of the $K\beta/Ka$ ratio has been observed for Y_2S_3. We found a general increase of the $K\beta/Ka$ intensity ratios for different compounds. This situation is more complex because the $K\beta/Ka$ intensity ratio is affected by the chemical bonding type, (ionic, metallic, covalent), the individual characteristics of the structure of molecules, complexes and crystals (polarity, valency and electronegativity of atoms, co-ordination number, ionicities of covalent bond etc.).

We found that the chemical effect on the $K\beta/Ka$ ratios for 4d elements is small but the dependence of the $K\beta_2/Ka$ ratios on the chemical environments is appreciable. This can be understood by the fact that in 4d elements the valance state consists of the 4d, 5s and 5p electrons and the influence of the chemical state on the $K\beta_{1,3}$ (3p→1s) X-ray emission is negligible. Yamoto et al. (1986) found similar results for compounds involving Tc isotopes and Mukoyoma et al. (2000) found similar results theoretically for Mo and Tc compounds.

The overall error in the present measurements is estimated to be 3-8%. This error is attributed to the uncertainties in different parameters used to determine the $K\beta_1/Ka$, $K\beta_2/Ka$, $K\beta_2/K\beta_1$ and $K\beta/Ka$ values; such as, $I_0G\varepsilon$ product (1.0-2.5%), in the absorption correction factor (0.3-1.5%), the error in the area evaluation under the Ka, $K\beta_1$, $K\beta_2$ and $K\beta$ X-ray peak (0.5-3.0%) and the other systematic errors (1.0-2.0%).

4. Conclusion

There has been increasing interest in chemical speciation of the elements in recent years which can be attributed to the great alterations in the chemical and biological properties of the elements depending on their oxidation state, the type of chemical bonds etc. Usually, the influence of the chemical environment results in energy shifts of the characteristic X-ray lines, formation of satellite lines and changes in the emission linewidths and relative X-ray intensities. High resolution X-ray spectroscopy, employing crystal spectrometers of a few eV resolutions, can be applied to probe these phenomena efficiently, exploiting them for chemical state analysis. Measurements of the shapes and wavelengths of certain X-ray lines have been made by previous investigators with both EDXRF and WDXRF. It has been shown that the WDXRF spectrometer is capable of measuring X-ray wavelengths with a precision equal to or greater than that attained with the EDXRF system. Both EDXRF and WDXRF technique has been used to study the effect of chemical state of an element on characteristic X-rays.

We have presented and discussed the effect of chemical composition and external magnetic field on the $K\beta_{1,3}/Ka$, $K\beta_{2,4}/Ka$, $K\beta_{2,4}/K\beta_{1,3}$ and $K\beta/Ka$ intensity ratios for some Yttrium compounds. The experimental measurements have been performed with a Si(Li) detector. The observed spectral features, namely the asymmetry indices, FWHM values, chemical shifts, energy separations between Ka and $K\beta$ lines and $K\beta/Ka$ intensity ratio values show an interesting correlation with crystal symmetries. Furthermore, these values change

symmetrically with the external magnetic field. There is a relation between the crystal structures and *K* X-ray emission rate because of the change in bond distance, inter atomic distance, the interaction between ligand atoms and the central atom, and the Auger electron and dipole transition. These situations cause a redistribution of the electron configuration in the molecule.

A correlation between the $K\beta/Ka$ intensity ratio of 4d elements and chemical state was found in this work. Excluding the values for Y, we can generally state that $K\beta/Ka$ intensity ratio increases for different compounds. The $K\beta_1/Ka$, $K\beta_2/Ka$, $K\beta_2/K\beta_1$ and $K\beta/Ka$ intensity ratio values were obtained in the present work and listed in Table 6 and compared with other experimental and theoretical values. As a result, we can say that the uncertainties of the measured values are too large to allow any statement about the specific dependence of the $K\beta/Ka$ intensity ratio on the crystal symmetry, but small enough to show significant increase in the $K\beta/Ka$ intensity ratio with increasing external magnetic field values.

In general, our experimental values are qualitatively in agreement with the other experimental values. There are some differences between the results of this study and that of previous experimental work because these studies were carried out in different laboratories and different systems. We were not obtained researches interested in $K\beta_{1,3}/Ka$, $K\beta_{2,4}/Ka$, $K\beta_{2,4}/K\beta_{1,3}$ and $K\beta/Ka$ intensity ratio values for Y compounds. So we do not compare compounds these intensity ratio values in literature values. Rigorous systematic experiments and theoretical calculations are urgently needed for comparison with present experimental result. To obtain more definite conclusions on the magnetic field and crystal structure dependency of the atomic parameters, more experimental data are clearly needed, particularly for different symmetries and for chemical compounds.

5. Acknowledgment

This work was supported by the Scientific and Technological Research Council of Turkey (TUBITAK), under the project no 106T045.

6. References

Allinson, S.K. (1933). The Natural Widths of the *Ka* X-Ray Doublet from ^{26}Fe to ^{47}Ag. *Phys. Rev*. Vol.44, pp. 63-72.

Arndt, E.; Brunner, G. & Hartmann, E. (1982). *Kβ/Ka* Intensity Ratios for 3d Elements by Using Photoionisation and Electron Capture. *J. Phys. B*: *At. Mol. Opt. Phys*., Vol.15, pp. 887-889.

Balasubramanian, K. (1994). Relativistic Effects and Electronic Structure of Lanthanide and Actinide Molecules, in: Gschneidner, K.A.; Eyring, L.; Choppin, G.R. & Lander G.H. (Ed.), *Handbook of Physics and Chemistry of Rare Earth*, 18, Elsevier, Amsterdam, Chap. 119, pp. 29–50.

Band, I.M.; Kovtun, A.P.; Listengarten, M.A. & Trzhaskovskaya, M.B. (1985). The Effect of the Chemical Environment of Manganese and Chromium Atoms on the $K\beta/Ka$ X-Ray Intensity Ratio. *J. Electr. Spectr. and Relat. Phenom*., Vol.36, pp. 59-68.

Batrakov, Y.F.; Krivitsky, A.G. & Puchkova E.V. (2004). Relativistic Component of Chemical Shift of Uranium X-Ray Emission Lines. *Spectrochim. Acta Part B,* Vol.59, pp. 345 351.

Berenyi, D.; Hock, G.; Ricz, S.; Schlenk, B. & Valek, A. (1978). *Ka*/K*β X*-Ray Intensity Ratios and *K*-Shell Ionisation Cross Sections for Bombardment by Electrons of 300-600 keV. *J. Phys. B*, Vol.11, pp. 709-713.

Berger, M.J. & Hubbell, J.H. (1987). XCOM: Photon Cross-Sections on a Personnel Computer with (Version 1.2).

Brunner, G.; Nagel, M.; Hartmann, E. & Arndt, E. (1982). Chemical Sensitivity of the *Kβ/Ka* X-Ray Intensity Ratio for 3d Elements. *J. Phys. B*, Vol.15, pp. 4517-4522.

Demir, D. & Şahin, Y. (2006a). Measurement of the *K* shell X-Ray Production Cross-Sections and Fluorescence Yields for Nd, Eu, Gd, Dy and Ho using Radioisotopes X-Ray Fluorescence in the External Magnetic Field. *Eur. Phys. J. D,* Vol.44, pp. 34-38.

Demir, D. & Şahin, Y. (2006b). The Effect of an External Magnetic Field on the L_3 Subshell Fluorescence Yields and Level Widths for Gd, Dy, Hg and Pb at 59,54 keV. *Nucl. Instr. and Meth.*, Vol.254, pp. 43-48.

Deutsch, M. & Hart, M. (1982). Wavelength, Energy Shape, and Structure of the Cu Ka_1 X Ray-Emission Line. *Phys. Rev. B,* Vol.26, pp. 5558-5567.

Ertuğral, B.; Apaydın, G.; Çevik, U.; Ertuğrul, M. & Kopya, A.İ. (2007). *Kβ/Ka* X-Ray Intensity Ratios for Elements in the Range 16<Z<92 Excited by 5.9, 59.5 and 123.6 keV Photons. *Radiation Phys. and Chem.*, Vol.76, pp. 15-22.

Fichter, M. (1975). Das K-Röntgenemissionsspektrum von Phosphor in Abhängigkeit von der Chemischen Bindung. *Spectrochim. Acta Part B,* Vol.30, pp.417-431.

Giauque, R.D.; Goulding, F.S.; Jaklevic, J.M. & Pehl, R.H. (1973). Trace Element Determination with Semiconductor Detector X-Ray Spectrometers. *Anal. Chem.*, Vol.45, pp. 671-681.

Gohshi, Y. & Ohtsuka, A. (1973). The Application of Chemical Effects in High Resolution X-Ray Spectrometry. *Adv. X-Ray Anal.*, Vol. 28, pp. 179-188.

Gohshi, Y.; Hirao, O. & Suzuki, I. (1975). Chemical State Analysis of Sulfur, Chromium and Tin by High Resolution X-Ray Spectrometry. *Adv. X-Ray Anal.*, Vol.18, pp. 406-414.

Groot, F.M.F. (1994a). X-Ray Absorption and Dichroism of Transition Metals and Their Compounds. *J. Electron Spectrosc. Relat. Phenom.*, Vol.676, pp. 529-622.

Groot, F.M.F. (1994b). New Directions in Research with Third-Generation Soft X-Ray Synchrotron Radiation Sources. *Applied Sciences*, Vol.254.

Han, I.; Porikli, S.; Şahin, M. & Demir. D. (2010). Measurementof *La*, *Lβ* and Total *L* X-ray Fluorescence Cross-Sections for Some Elements with 40<Z<53. *Radiation Physics and Chemistry,* Vol.79, pp. 393–396.

Iiahara, J.; Omorr, T., Yoshihara, K.; & Ishii, K. (1993). Chemical Effects on Chromium *L* X-Rays. *Nucl. Instr. Methods. B,* Vol.73, pp. 32-34.

Kataria, S.K.; Govil, R.; Saxena, A. & Bajpei, H.N. (1986). Chemical Effects in X-ray Fluorescence Analysis. *X-Ray Spectr.*, Vol.15, pp. 49-53.

Katz, J.J.; Seaborg, G.T. & Morss, L.R. (1986). 2nd ed, The Chemistry of the Actinide Elements, 2, *Chapman and Hall*, New York, pp. 1131–1165.

Khan, M.R. & Karimi, M. (1980). *Kβ/Ka* Ratıos ın Energy-Dispersive X-Ray Emission Analysis. *X-Ray Spectrom*., Vol.9, pp. 32-35.

Krause, M.O. (1979). Atomic Radiative and Radiationless Yields for *K* and *L* Shells. *Chem. Ref. Data*., Vol.8, pp. 307-327.

Küçükönder, A.; Şahin, Y.; Büyükkasap, E. & Kopya, A. (1993). Chemical effect on *Kβ/Ka* X Ray Intensity Ratios in Coordination Compounds of Some 3d Elements. *J. Phys. B*: *At. Mol. Opt. Phys*., Vol.26, pp. 101-105

Leonhardt, G. & Meisel, A. (1970). Determination of Effective Atomic Changes From the Chemical Shifts of X-Ray Emission Lines. *J. Chem. Phys*. Vol.52, pp. 6189-6198.

Makarov, L.L. (1999). X-ray Emission Effects as a Tool to Study Light Actinides. *Czech. J. Phys*., Vol.49, pp. 610–616.

Manson, S. T. (1974). X-Ray Emission Rates in the Hartree–Slater Approximation. *At. Data Nucl. Data Tables*. Vol.14, pp. 111-120.

Meisel, A.; Leonhardt, G. & Szargan, R. (1989). X-Ray Spectra and Chemical Binding, *Chemical Physics*, Vol.37, edited by F.P. Schafer, V.I. Goldanskii & J.P. Toennies (Springer-Verlag, Berlin).

Mukoyoma, T.; Taniguchi, K. & Adachi, H. (1986). Chemical Effect on *Kβ/Ka* X-Ray Intensity Ratios. *Phys. Rev. B*, Vol.34, pp. 3710-3716.

Mukoyoma, T.; Taniguchi, K. & Adachi, H. (2000). Variation of *Kβ/Ka* X-Ray Intensity Ratios in 3d elements. *X-Ray Spectr*., Vol.29, pp. 426-429.

Mukoyama, T. (2004). Theory of X-ray Absorption and Emission Spectra. *Spectrochim. Acta Part B*, Vol.59, pp. 1107-1115.

Nagel, D.J. & Baun, W.L. (1974). In: L.V. Azaroff (Ed.), *X-Ray Spectroscopy*, McGraw-Hill, US, Ch. 9.

Padhi , H.C.; Bhuinya, C.R. & Dhal, B.B. (1993). Influence of Solid-State Effects on the *Kβ/Ka* Intensity Ratios of Ti and V in TiB_2, VB_2 and VN. *J. Phys. B*: *At. Mol. Opt. Phys*., Vol.26, pp. 4465-4469.

Padhi , H.C. & Dhal, B.B. (1995). *Kβ/Ka* X-Ray-Intensity Ratios of Fe, Co, Ni, Cu, Mo, Ru, Rh and Pd in Equiatomic Aluminides. *Solid State Commun*., Vol. 96, pp. 171-173.

Paic, G. & Pecar, V. (1976). Study of Anomalies in *Kβ/Ka* Ratios Observed Following *K* Electron Capture. *Phys. Rev. A*, Vol.14, pp. 2190-2192.

Pepper, M. & Bursten, B.E. (1991). The Electronic Structure of Actinide Containing Molecules: a Challenge to Applied Quantum Chemistry. *Chem. Rev.,* Vol.91, pp. 719–741.

Porikli, S. & Kurucu, Y. (2008a). The Effect of an External Magnetic Field on the *Ka* and *Kβ* X-Ray Emission Lines of the 3*d* Transition Metals. *Instr. Science and Tech*., Vol.36:4, pp. 341-354.

Porikli, S. & Kurucu, Y. (2008b). Effects of the External Magnetic Field and Chemical Combination on *Kβ/Ka* X-Ray Intensity Ratios of Some Nickel and Cobalt Compounds. *Appl. Rad. and Isot*., Vol.66, pp. 1381-1386.

Porikli, S.; Demir, D. & Kurucu, Y. (2008c). Variation of *Kβ/Ka* X-Ray Intensity Ratio and Lineshape with the Effects of External Magnetic Field and Chemical Combination. *Eur. Phys. J. D,* Vol.47, pp. 315–323.

Porikli, S.; Han, İ.; Yalçın, P. & Kurucu, Y. (2011a). Determination of Chemical Effect on the $K\beta_1/Ka$, $K\beta_2/Ka$, $K\beta_2/K\beta_1$ and $K\beta/Ka$ X-Ray Intensity Ratios of 4d Transition Metals. *Spectroscopy Letters*, Vol.44, pp. 38–46.

Porikli, S. (2011b). Influence of the Chemical Environment Changes on the Line Shape and Intensity Ratio Values for La, Ce and Pr L Lines *Spectra. Chem. Phys. Lett.*, Vol.508, pp. 165-170.DOI information: 10.1016/j.cplett.2011.04.021

Pyykko, P. (1988). Relativistic Effects in Structural Chemistry. *Chem. Rev.,* Vol.88, pp. 563-94.

Raj, S.; Padhi, H.C. & Polasik, M. (1998). Influence of Chemical Effect on the *Kβ*-to-*Ka* X-Ray Intensity ratios of Ti, V, Cr, and Fe in TiC, VC, CrB, CrB_2 and FeB. *Nucl. Instrum. Meth. in Phys. Res. B,* Vol.145, pp. 485–491.

Rao, N.V.; Reddy, S.B; Satyanarayana, G. & Sastry, D.L. (1986). *Kβ/Ka* X-Ray Intensity Ratios. *Physica C*, Vol.142, pp. 375-380.

Salem, S.I.; Panossian, S.L. & Krause, R.A. (1974). Quantum Mechanics of Atomic Spectra and Atomic Structure. *At. Data Nucl. Data Tables*, Vol.14, pp.91-109.

Scofield, J.H. (1969). Radiative Decay Rates of Vacancies in *K* and *L* Shells. *Phys. Rev.*, Vol.179, pp. 9-16.

Scofield, J.H. (1973). Theoretical Photoionization Cross Sections from 1 to 1500 keV, Unpublished *Lawrence Livermore Laboratory Report* UCRL-51326, Livermore, California

Scofield, J.H. (1974a). Relativistic Hartree–Slater Values for *K* and *L* Shell X-Ray Emission Rates. *Atomic Data and Nuclear Data Tables*, Vol.14, pp. 121-137.

Scofield, J.H. (1974b). Exchange Corrections of *K* X-ray Emission Rates. *Phys. Rev. A*, Vol.9, pp. 1041–1049.

Stöhr, Y. & Wu, Y. (1994). X-Ray Magnetic Circular Dichroism: Basic Concepts and Theory for 3d Transition Metal Atoms. *New Directions in Research with 3rd Generation Soft X-Ray Synchrotron Radiation Sources*, Editors F. Schlachter and F. Wuilleumier (Kluwer, Netherlands, 1993), p. 221.

Tamaki, Y.; Omori, T. & Shiokawa, T. (1979). Chemical Effect on the *Kβ/Ka* Intensity Ratios of the Daughter Atoms Formed by the EC decay of ^{51}Cr and ^{54}Mn. *Radiochem. Radioanal. Lett.*, Vol.37, pp. 39-44.

Taniguchi, K. (1984). Chemical-State Analysis by Means of Soft X-Ray Spectroscopy. 2. *Kβ* Spectra for Phosphorus, Sulfur, and Chlorine in Various Compounds. *Bull. Chem. Soc. Jpn.*, Vol.57, pp. 915-920.

Thole, B.T.; Carra, P.; Sette, F. & Van der Lean, G. (1992). X-Ray Circular-Dichroism as a Probe of Orbital Magnetization. *Phys. Rev. Lett.*, Vol.68, pp. 1943-1946.

Torres Deluigi, M.; Perino, E.; Olsina R. & Riveros de la Vega, A. (2003). Sulfur and Phosphorus *Kβ* Spectra Analyses in Sulfite, Sulfate and Phosphate Compounds by X-Ray Fluorescence Spectrometry. *Spectrochim. Acta Part B,* Vol.58, pp- 1699-1707.

Urch, D.S. (1979). Theory, Techniques, and Application; Brundle, C. R., Baker, A. D., Eds.; Academic Press: New York, *Electron Spectrosc.*, Vol.3, pp. 1-39.

Yamoto, I.; Kaji, H. & Yoshihara, K. (1986). Studies on Chemical Effects on X-Ray Intensity Ratios of *Kβ/Ka* in Nuclear Decay of Technetium Nuclides ^{99m}Tc, ^{97m}Tc and ^{95m}Tc. *J. Chem. Phys.*, Vol.84, pp- 522-527.

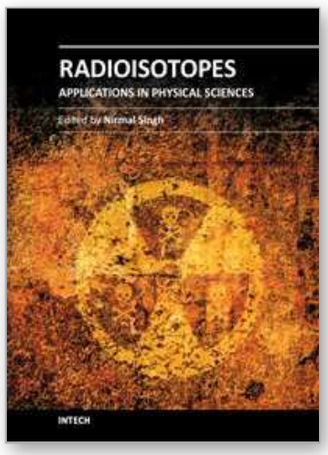

Radioisotopes - Applications in Physical Sciences

Edited by Prof. Nirmal Singh

ISBN 978-953-307-510-5
Hard cover, 496 pages
Publisher InTech
Published online 19, October, 2011
Published in print edition October, 2011

The book Radioisotopes - Applications in Physical Sciences is divided into three sections namely: Radioisotopes and Some Physical Aspects, Radioisotopes in Environment and Radioisotopes in Power System Space Applications. Section I contains nine chapters on radioisotopes and production and their various applications in some physical and chemical processes. In Section II, ten chapters on the applications of radioisotopes in environment have been added. The interesting articles related to soil, water, environmental dosimetry/tracer and composition analyzer etc. are worth reading. Section III has three chapters on the use of radioisotopes in power systems which generate electrical power by converting heat released from the nuclear decay of radioactive isotopes. The system has to be flown in space for space exploration and radioisotopes can be a good alternative for heat-to-electrical energy conversion. The reader will very much benefit from the chapters presented in this section.

How to reference

In order to correctly reference this scholarly work, feel free to copy and paste the following:

Sevil Porikli and Yakup Kurucu (2011). Determination of Chemical State and External Magnetic Field Effect on the Energy Shifts and X-Ray Intensity Ratios of Yttrium and Its Compounds, Radioisotopes - Applications in Physical Sciences, Prof. Nirmal Singh (Ed.), ISBN: 978-953-307-510-5, InTech, Available from: http://www.intechopen.com/books/radioisotopes-applications-in-physical-sciences/determination-of-chemical-state-and-external-magnetic-field-effect-on-the-energy-shifts-and-x-ray-in

INTECH
open science | open minds

InTech Europe
University Campus STeP Ri
Slavka Krautzeka 83/A
51000 Rijeka, Croatia
Phone: +385 (51) 770 447
Fax: +385 (51) 686 166
www.intechopen.com

InTech China
Unit 405, Office Block, Hotel Equatorial Shanghai
No.65, Yan An Road (West), Shanghai, 200040, China
中国上海市延安西路65号上海国际贵都大饭店办公楼405单元
Phone: +86-21-62489820
Fax: +86-21-62489821

IntechOpen